

Technical Note

Very Local Subsidence Near the Hot Spring Region in Hakone Volcano, Japan, Inferred from InSAR Time Series Analysis of ALOS/PALSAR Data

Ryosuke Doke * , George Kikugawa and Kazuhiro Itadera

Hot Springs Research Institute of Kanagawa Prefecture, 586 Iriuda, Odawara 250-0031, Japan; kikugawa@onken.odawara.kanagawa.jp (G.K.); itadera@onken.odawara.kanagawa.jp (K.I.)

* Correspondence: r-doke@onken.odawara.kanagawa.jp; Tel.: +81-465-23-3588

Received: 28 July 2020; Accepted: 31 August 2020; Published: 1 September 2020



Abstract: Monitoring of surface displacement by satellite-based interferometric synthetic aperture radar (InSAR) analysis is an effective method for detecting land subsidence in areas where routes of leveling measurements are undeveloped, such as mountainous areas. In particular, InSAR-based monitoring around well-developed hot spring resorts, such as those in Japan, is useful for conserving hot spring resources. Hakone Volcano is one of the major hot spring resorts in Japan, and many hot spring wells have been developed in the Owakudani fumarole area, where a small phreatic eruption occurred in 2015. In this study, we performed an InSAR time series analysis using the small baseline subset (SBAS) method and ALOS/PALSAR scenes of the Hakone Volcano to monitor surface displacements around the volcano. The results of the SBAS-InSAR time series analysis show highly localized subsidence to the west of Owakudani from 2006–2011 when the ALOS/PALSAR satellite was operated. The area of subsidence was approximately 500 m in diameter, and the peak rate of subsidence was approximately 25 mm/year. Modeling using a point pressure source suggested that the subsidence was caused by a contraction at approximately 700 m above sea level (about 300 m below the ground surface). The rate of this contraction was estimated to be $1.04 \times 10^4 \text{ m}^3/\text{year}$. Hot spring water is collected from a nearby well at almost the same depth as the contraction source, and its main dissolved ion component is chloride ions, suggesting that the hydrothermal fluids are supplied from deep within the volcano. The land subsidence suggests that the fumarole activity is attenuating due to a decrease in the supply of hydrothermal fluids from deeper areas.

Keywords: InSAR; ALOS/PALSAR; time series analysis; SBAS; land subsidence; hot spring water; hydrothermal fluids; Hakone Volcano

1. Introduction

Land subsidence due to the over-extraction of groundwater needs to be carefully monitored as it can lead to the destruction of buildings and infrastructure in urban areas. In Japan, land subsidence is monitored by leveling [1]. Although leveling measurements can be used to precisely determine vertical displacements, they can only be used to monitor displacements if benchmarks have been installed; if local subsidence occurs in areas away from benchmarks, it may be overlooked. Consequently, conventional leveling measurements are not very effective for detecting land subsidence in mountainous areas where leveling routes are not well developed. There are numerous volcanoes in Japan, many of which have hot springs and are popular tourist destinations. Large-scale resort development has occurred in these mountainous areas, which has meant that extensive drilling for new sources of hot spring water has occurred. Therefore, it is important to monitor land subsidence in mountainous areas with many large spa resorts, not only to maintain the infrastructure, but also to conserve hot spring resources.

Interferometric synthetic aperture radar (InSAR) analysis, using satellite-based sensors, is one of the most effective tools for detecting unknown land subsidence [2]. While InSAR is less precise than conventional leveling measurements, the technique does not require a network of ground-based observations. In addition, InSAR analysis is well suited for application in mountainous areas, where there is no existing observation network. SAR satellites were launched by governments and private companies, primarily to monitor the natural and physical characteristics of the Earth, including vegetation, natural resources, and crustal deformation for disaster monitoring. Various wavelengths are used for land surface observations, ranging from the L-band to the X-band, depending on specific requirements. InSAR analysis using short-wavelength sensors (e.g., X-band and C-band) generally does not provide good coherence in forested areas, which makes it challenging to monitor ground movement. Conversely, InSAR analyses using long-wavelength (L-band) sensors can achieve good coherence, even in forested areas, enabling users to monitor ground deformation. It is therefore considered that monitoring by L-band sensors will play an important role in clarifying ground deformation in mountainous areas in places such as forested area of Japan.

The Hakone Volcano (Figure 1), located in the plate collision zone of the Izu Peninsula with Japan mainland [3], has been active for approximately 400,000 years and is one of several active volcanoes in Japan. Hakone is a caldera volcano with a complex of stratovolcanoes of basaltic to andesitic composition forming the caldera rim (≥ 230 ka) (Figure 2) [4]. Within the last 37,000 years, andesitic eruptive activity has formed a central cone of the volcano [4]. The latest magmatic eruption occurred about 3000 years ago on the northern slope of the central cone and caused a sector collapse that formed an amphitheater [4]. Owakudani, the largest fumarole area of the volcano, is located at the eastern margin of the amphitheater (Figure 3). In the Owakudani, hot spring water is artificially produced from the self-discharged volcanic steam that comes up from borehole (steam wells), which are several hundred meters in depth. Total heat flux of natural fumaroles and steam wells added together was estimated to be approximately 15 to 20 MW from 1983 to 2012, and it dropped in recent years [5]. The recent activity of the volcano started around the year 2000, and a small-scale phreatic eruption occurred in Owakudani in 2015 [5]. Hakone Volcano is located approximately 100 km west of Tokyo (Figure 1), the capital of Japan. The region surrounding the volcano has a well-developed infrastructure, comprising railways, roads, hotels, and other recreational amenities. It is a major hot-spring tourism destination in Japan that is visited by approximately 20 million tourists a year.

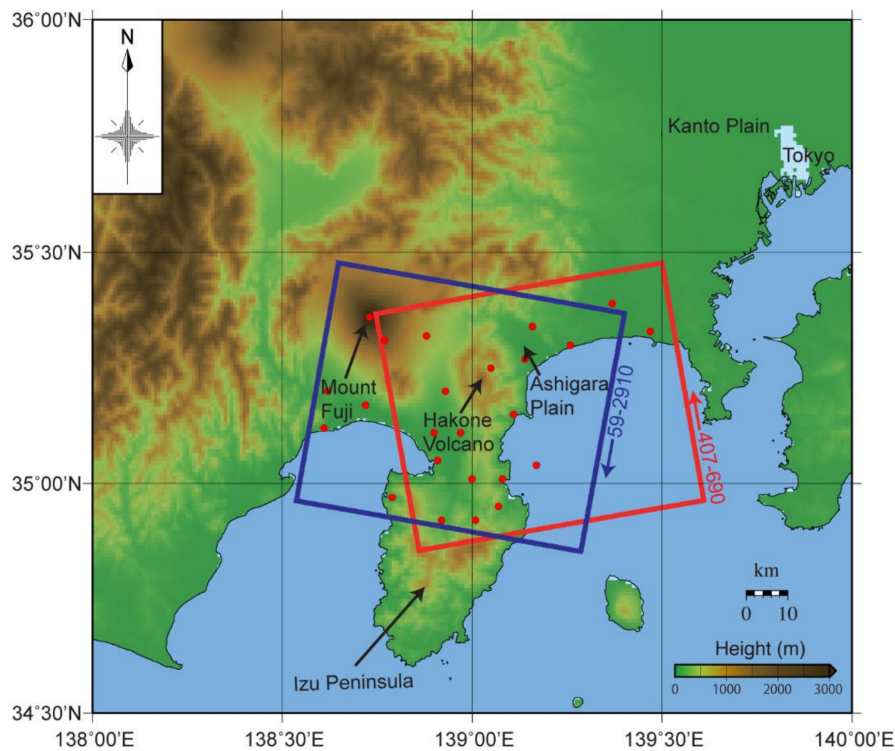


Figure 1. Map showing the area around Hakone Volcano. The topographical map is based on 50 m mesh height data released by the Geospatial Information Authority of Japan (GSI). The red and blue rectangles show the area included in the scenes of the ascending and descending orbits, respectively. Red points show the location of ground control points used for the analysis.

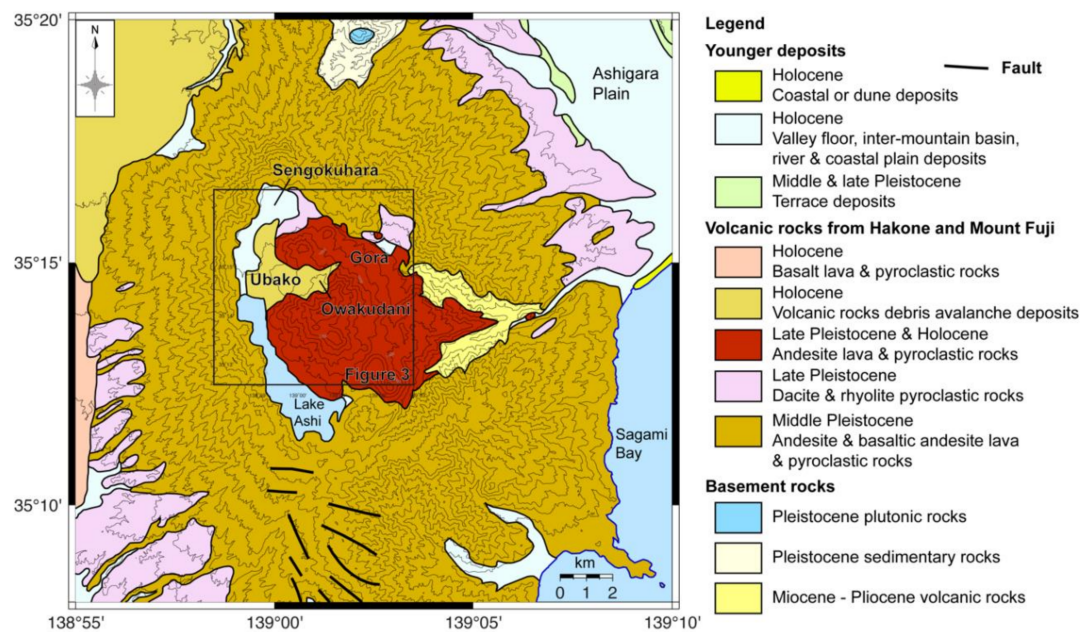


Figure 2. Geological map around Hakone Volcano (modified from the Seamless Geological map of Japan [6]). The original geological map was simplified based on ages and types of rocks. Contour lines in which intervals are 100 m were extracted from 10 m mesh height data released by the GSI. The area enclosed by the rectangle indicates the focus area of this study (Figure 3).

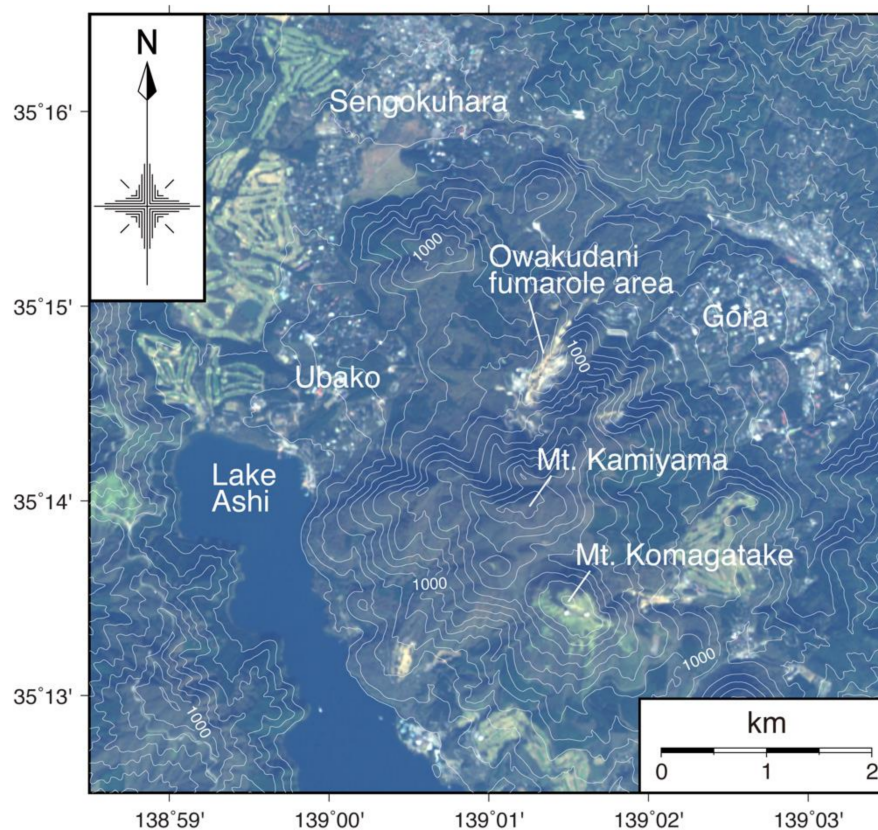


Figure 3. Location map of the focused area of this study. The base map is a true-color image captured by ALOS/AVNIR-2 on 10 November 2006. Contour lines in which intervals are 50 m were extracted from 10 m mesh height data released by the GSI.

Based on seismic activity and InSAR analyses, the occurrence of the phreatic eruptions of Hakone Volcano and its associated seismic swarm activities are thought to be related to hydrothermal activity in the shallow parts of the volcano [7,8]. It is considered that this activity is closely related to the formation of hot spring water [9]. It is therefore considered important to clarify the reasons for ground deformation in this area, not only for preventing a volcanic disaster, but also to better understand the formation mechanism of hot springs in Hakone Volcano and the conservation of hot spring resources.

In this study, we performed an InSAR time series analysis using the small baseline subset (SBAS) method [10], and data obtained from the Phased Array type L-band Synthetic Aperture Radar (PALSAR) aboard the Advanced Land Observing Satellite (ALOS). We detected highly localized subsidences in the fumarolic area, which is the principal hot spring area of Hakone.

2. Materials and Methods

We used data from the ALOS/PALSAR satellite launched by the Japan Aerospace Exploration Agency (JAXA), which has a wavelength of 23.6 cm (L-band). The satellite always observes the right side of the azimuth direction, and its revisit interval is 46 days [11]. ALOS/PALSAR was operated from 2006 to 2011, and its successor, ALOS-2/PALSAR-2, has been in operation since 2014. In this study, we obtained 24 scenes from Path 407-Frame 690 observed from the ascending orbit (observation from the western sky) and 22 scenes from Path 59-Frame 2910 observed from the descending orbit (observation from the eastern sky) which covers Hakone Volcano (Figure 1 and Table 1). The off-nadir angles for the scenes of both the ascending and descending orbits were 34.3°. The ALOS-2/PALSAR-2 data were not used in this study because the data acquisition interval was long, and the data available was insufficient for the analysis.

Table 1. Observation dates of scenes used for the interferometric synthetic aperture radar (InSAR) analysis in this study.

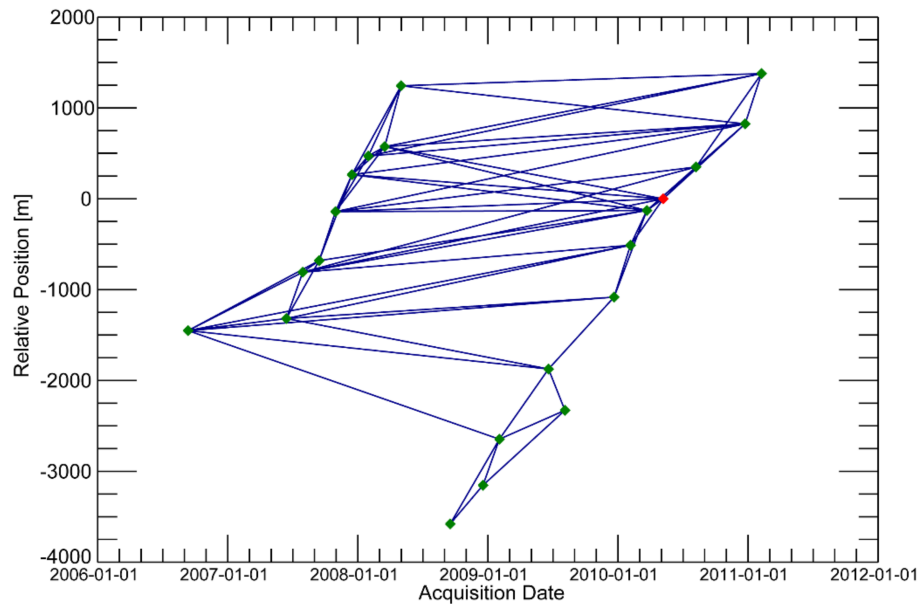
Ascending 407-690	Descending 59-2910
27 July 2006 ¹	29 September 2006
11 September 2006	14 November 2006
14 June 2007	30 December 2006
30 July 2007	17 August 2007
14 September 2007	02 October 2007 ²
30 October 2007	17 November 2007
15 December 2007	02 January 2008
30 January 2008	03 April 2008
16 March 2008	19 May 2008
01 May 2008	19 August 2008
16 June 2008 ¹	04 October 2008
01 August 2008 ¹	19 November 2008
16 September 2008	22 May 2009
17 December 2008	22 August 2009
01 February 2009	07 October 2009
19 June 2009	22 November 2009
04 August 2009	25 May 2010
20 December 2009	10 July 2010
04 February 2010	25 August 2010
22 March 2010	10 October 2010
07 May 2010 ²	25 November 2010
07 August 2010	12 April 2011 ¹
23 December 2010	
07 February 2011	

¹ Data excluded from the analysis. ² Data used as the super primary scene.

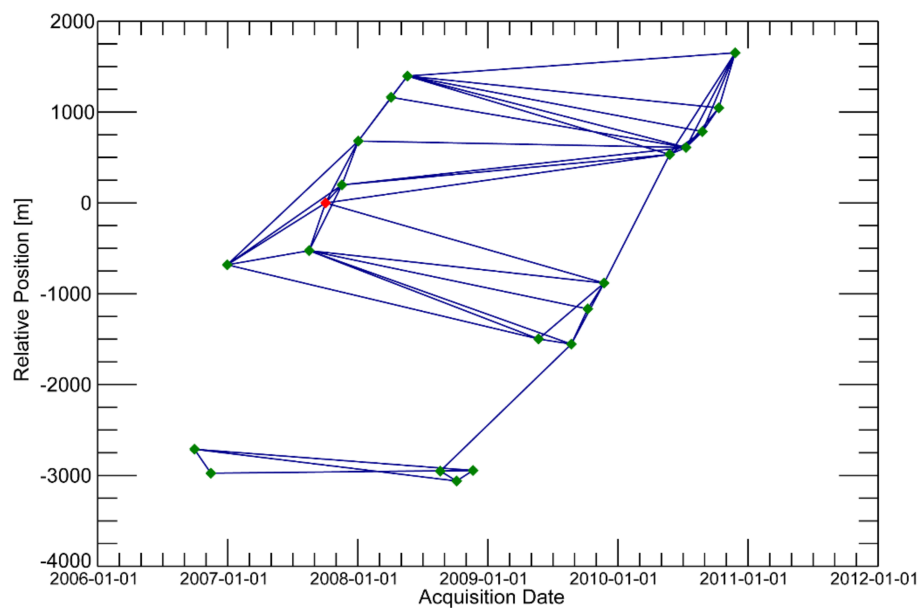
The ENVI+SARscape software program (Sarmap Sa, Caslano, Switzerland) was used for the SBAS-InSAR time series analysis in this study. Given that coherence is generally worse when the perpendicular baselines (Bperp) between ALOS/PALSAR orbits are more than 1000–1500 m, the analysis was conducted by extracting the interference pairs whose Bperp was less than approximately 1000 m. The pairs with weak interference were then removed visually, and 21 scenes-64 pairs in the ascending orbit and 21 scenes-57 pairs in the descending orbit were used for the analysis (Figure 4). Three of the scenes in the ascending orbit were excluded because of the large Bperp between the other scenes (Table 1). One of the scenes in the descending orbit was excluded because it was observed after the Tohoku-Oki Earthquake (M9.0) of 11 March 2011, and was affected by the earthquake displacement (Table 1).

To improve the signal-to-noise ratio, we averaged over approximately 15×15 m for each pixel in the azimuth and range directions. To remove the influence of topography in the initial interferogram, we used 10 m mesh elevation data obtained from the Geospatial Information Authority of Japan (GSI) and the geoid model of the Earth Gravitational Model 2008 [12]. The adaptive interferogram filtering algorithm [13] was applied to reduce the noise, and interferograms were unwrapped using the minimum cost flow approach [14]. During the time series inversion analysis, we used the global navigation satellite system (GNSS) of the GSI for establishing ground control points (GCPs) (Figure 1). The InSAR displacements were corrected with the displacements of the GCPs. For the GCPs, we used daily coordinates of GNSS sites published by the GSI and filtered these coordinate values in a 10-day time window. The velocity distributions obtained from the InSAR time series analysis were converted into a geographic coordinate system with an approximately 25×25 m mesh. Then, the velocity maps were obtained by masking pixels with a height estimation error of more than 5 m or a velocity estimation error of more than 8 mm/year. For the descending orbit, the data include Mount Fuji, which is the highest mountain in Japan (3776 m) and forms an independent peak with no continuity with the

surrounding mountains. Including Mount Fuji in the scene causes a large discrepancy between the displacements of GCPs and pixels in the InSAR time series analysis. However, when the western part of the scene, including Mount Fuji, was cropped, the displacements estimated by InSAR and the GCPs almost agreed. Therefore, we employed the result that excluded Mount Fuji.



(a)



(b)

Figure 4. Temporal and spatial baselines for the SBAS-InSAR analysis of ALOS/PALSAR data from the (a) ascending orbit, and the (b) descending orbit. Red points show the super primary scenes used for the analysis, which the software selected as the scene with the highest number of connections to other scenes.

3. Results

3.1. Ascending Orbit

Figure 5 shows the analysis results obtained for the ascending orbit (observations from the western sky). The colors of the figures show the satellite line-of-sight (LOS) velocity; the positive values shown in red indicate the LOS velocity toward the satellite, while the negative values shown in blue indicate the LOS velocity away from the satellite. Since the LOS velocities are corrected by GNSS displacements, these are not relative, but absolute velocities. A LOS velocity of approximately 4 mm/year toward the satellite was observed over the entire area (Figure 5a). A maximum LOS velocity of about 23 mm/year away from the satellite was observed to the west of Owakudani (Figure 5b), the largest fumarole area in the Hakone Volcano.

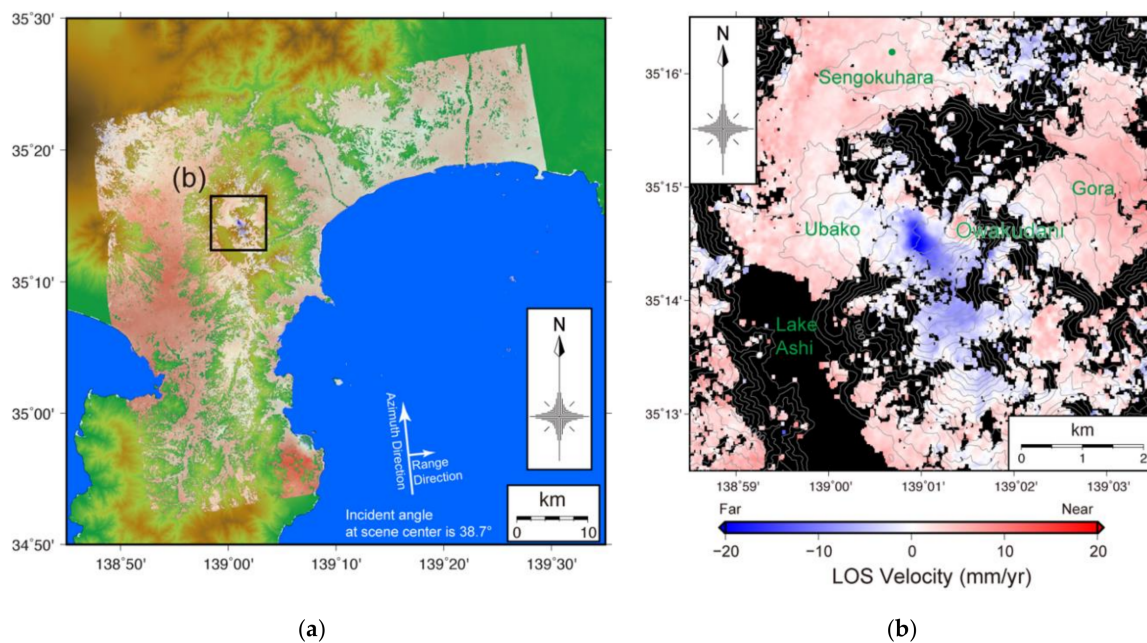


Figure 5. Distribution of line-of-sight (LOS) velocity in the ascending orbit for the (a) entire region; (b) area of interest shown in the black rectangle (inset) in (a). The base map of (a) is a topographical map based on 10 m mesh height data released by the GSL, and its color scale is the same as Figure 1. Intervals of contour lines in (b) are 50 m in height.

3.2. Descending Orbit

Figure 6 shows the results of the analysis for the descending orbit (observation from the eastern sky). A LOS velocity of about 4.5–5.8 mm/year away from the satellite was observed over almost the entire area (Figure 6a). In the areas around Hakone Volcano and Mount Fuji, LOS velocities toward the satellite (about 0–7 mm/year) were observed (Figure 6a). A maximum LOS velocity of about 16 mm/year away from the satellite was observed to the west of Owakudani (Figure 6b).

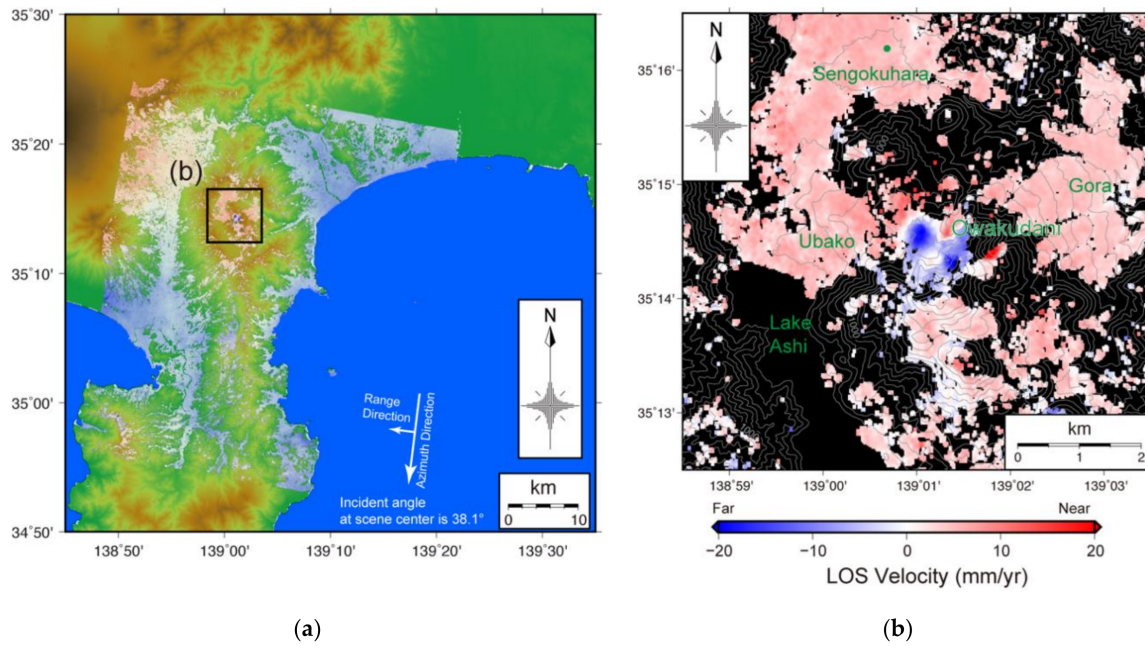


Figure 6. Distribution of LOS velocity in the descending orbit for the (a) entire region; (b) area of interest shown in the black rectangle (inset) in (a). The base map of (a) is a topographical map based on 10 m mesh height data released by the GSI, and its color scale is the same as Figure 1. Intervals of contour lines in (b) are 50 m in height.

3.3. 2.5-D Analysis

The LOS velocities obtained for ascending and descending orbits were transformed to the velocities of the quasi-eastward and quasi-upward components by applying 2.5-D analysis [15]. Quasi-eastward and quasi-upward velocities (V_{QE} , V_{QU}) are estimated from LOS velocity in ascending and descending orbits (V_A , V_D), and these unit vectors (\vec{A} , \vec{D}) by following equations.

A normal vector \vec{N} (x , y , z) of the LOS plane created by both LOS vectors are estimated as follows:

$$\vec{N} = \vec{A} \times \vec{D} \tag{1}$$

A line vector where the LOS plane and horizontal plane intersect is represented as \vec{L} (y , $-x$, 0), and its magnitude is as follows:

$$|\vec{L}| = \sqrt{x^2 + y^2} \tag{2}$$

Angles (θ_A , θ_D) between \vec{L} and LOS vectors (\vec{A} , \vec{D}) are estimated as follows:

$$|\vec{L}| \cos \theta_A = \vec{A} \cdot \vec{L} \tag{3}$$

$$|\vec{L}| \cos \theta_D = \vec{D} \cdot \vec{L} \tag{4}$$

Quasi-eastward and quasi-upward velocities (V_{QE} V_{QU}) are estimated as follows:

$$\begin{pmatrix} V_A & V_D \end{pmatrix} = \begin{pmatrix} V_{QE} & V_{QU} \end{pmatrix} \begin{pmatrix} \cos \theta_A & \cos \theta_D \\ \sin \theta_A & \sin \theta_D \end{pmatrix} \tag{5}$$

The strike and dip of the LOS plane varied slightly from point to point, but these were approximately 269° and 85° , respectively.

The quasi-eastward velocity shows that almost the entire area was displaced westward (Figure 7a). This westward displacement is considered to be a regional tectonic displacement caused by the Pacific Plate, which is subducting beneath the northeastern Japan [16,17]. On the other hand, the areas near Mount Fuji and Hakone Volcano showed eastward velocities (Figure 7a,b). Since expansions of volcanic edifices were observed by GNSS around Mount Fuji and Hakone Volcano during the study period [18,19], the eastward velocities might be consistent with the GNSS displacements.

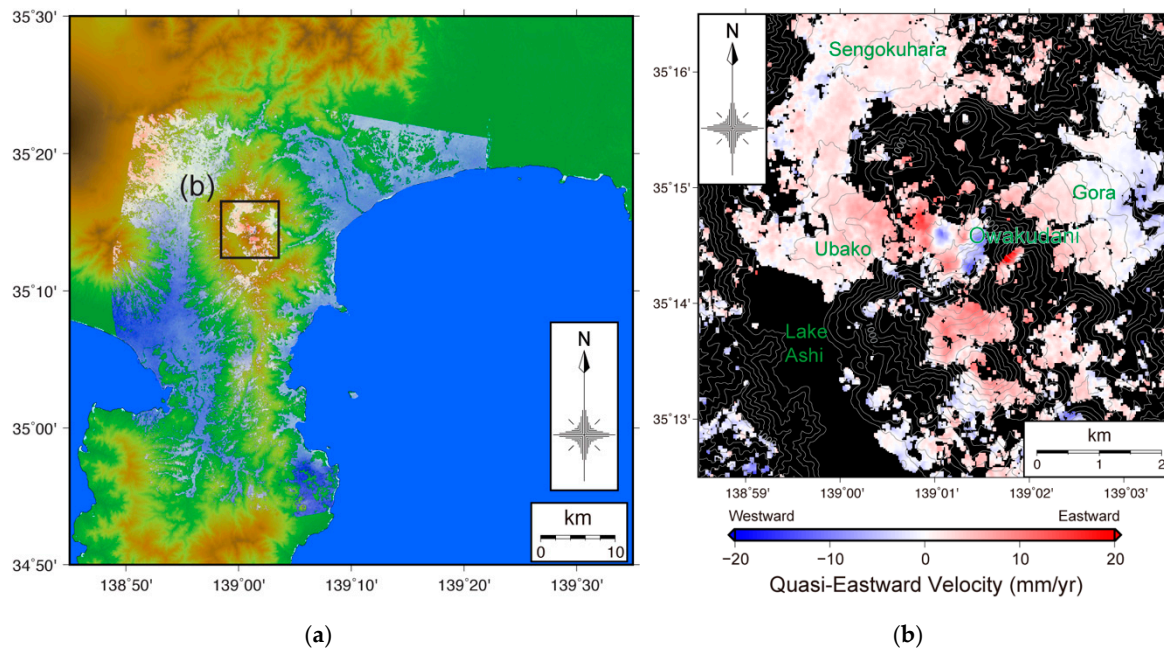


Figure 7. Distribution of quasi-eastward velocity over the (a) entire region; (b) area of interest shown in the black rectangle (inset) in (a). The base map of (a) is a topographical map based on 10 m mesh height data released by the GSI, and its color scale is the same as Figure 1. Intervals of contour lines in (b) are 50 m in height.

The quasi-upward velocity findings showed that the areas around Mount Fuji, Hakone Volcano, and the Izu Peninsula were uplifted, and the Ashigara Plain, located to the east of Hakone Volcano, subsided slightly (Figure 8a). These displacements are thought to be caused by tectonic deformations by the Izu Peninsula colliding with the main part of the Japanese Islands [3] and volcanic activities [18,19]. To the west of Owakudani, where volcanic rock debris-avalanche deposits are distributed on the surface (Figure 2), a maximum subsidence rate of about 25 mm/year was observed within an area with a diameter of about 500 m (Figure 8b). The displacement appears to have progressed at a constant rate over the observation period (Figure 9). Moreover, regarding the quasi-eastward component, both sides of the center of the subsidence area were displaced inwards; that is, the western side was displaced eastward, and the eastern side was displaced westward (Figure 7b). This result indicates that contractional displacement was dominant to the west of Owakudani.

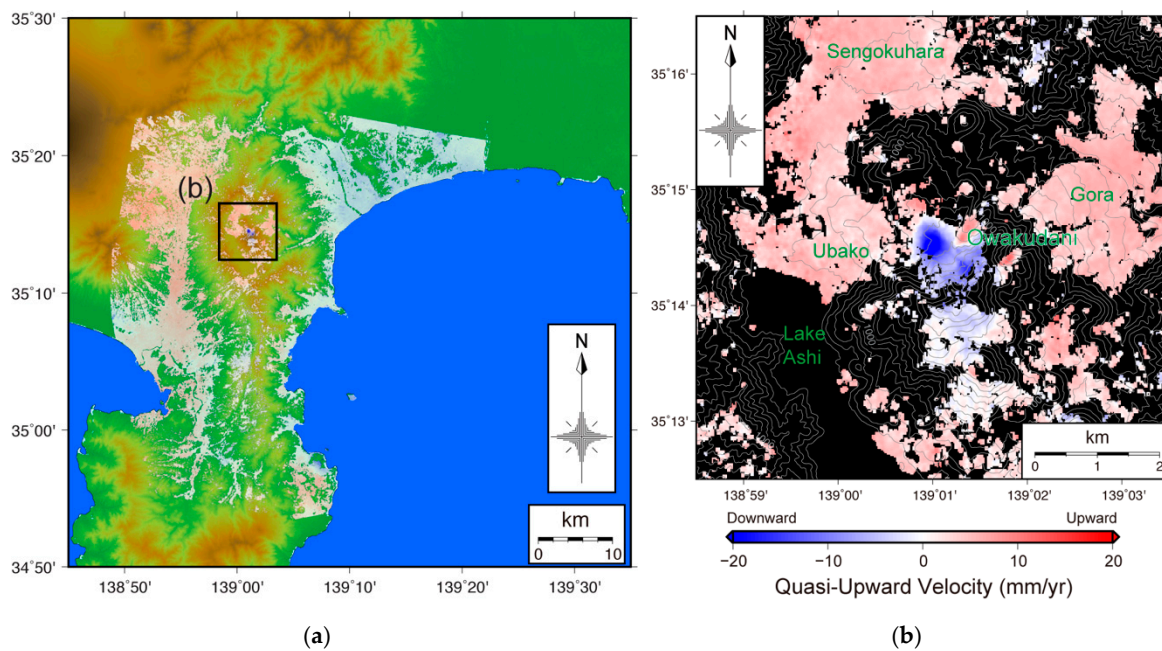


Figure 8. Distribution of quasi-upward velocity over the (a) entire region; (b) area of interest shown in the black rectangle (inset) in (a). The base map of (a) is a topographical map based on 10 m mesh height data released by the GSI, and its color scale is the same as Figure 1. Intervals of contour lines in (b) are 50 m in height.

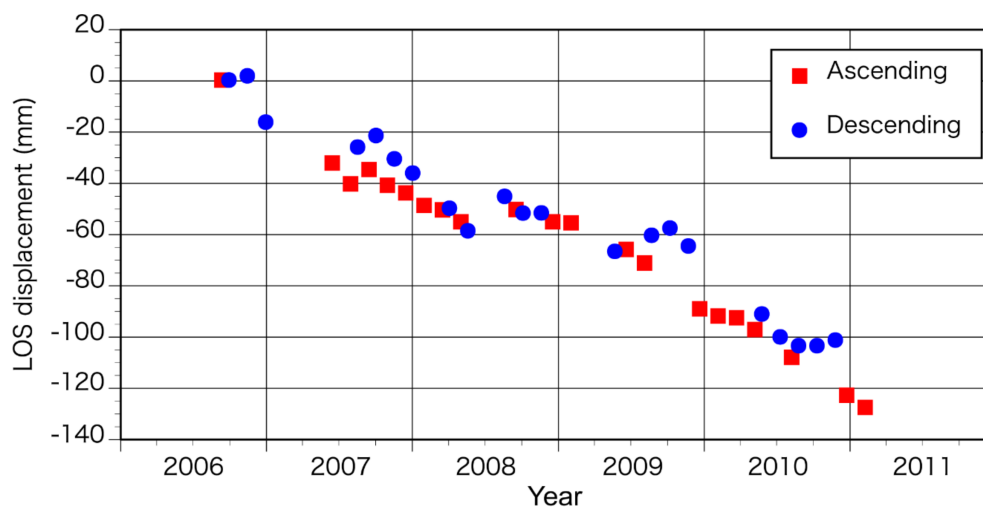


Figure 9. Time variation of displacement in pixels where the maximum velocities were observed to the west of Owakudani. Displacements were obtained by subtracting the displacement of an arbitrarily selected reference point near Sengokuhara (the green points in Figures 5b and 6b) to remove the displacement around the Hakone Volcano.

3.4. Modeling

Since the contractional displacements are dominant, we used a model involving a point pressure source in an elastic half-space body [20] to explain the subsidence to the west of Owakudani. A modeling tool in ENVI+SARscape, which implements inversion of the Levenberg–Marquardt least-squares approach [21], was used to estimate the volume variation and 3-D position of the pressure source. During the inversion analysis, the influence of topography was compensated for by the elevation data. Moreover, the offset parameters of the InSAR images were also estimated to consider the LOS velocity around the Hakone Volcano. After the optimum values of the model parameters were obtained by the

inversion, the variations in the residual root mean square (RMS) values were obtained by forward modeling with varying parameters (i.e., altitude and volume variation) to validate the sensitivities of each parameter.

The modeling results show that the subsidence can be explained by a point pressure source contracting at a rate of $1.04 \times 10^4 \text{ m}^3/\text{year}$ at the height of about 700 m above sea level (about 300 m below the ground surface) just under the area of subsidence (Table 2 and Figure 10). Based on the residual RMS values (Figure 11) estimated by the forward modeling, the parameters of the model are considered well-constrained, especially with respect to altitude. For example, a residual RMS value of 4 mm or less would be achieved at an altitude of 620–750 m and a volume variation of -1.4×10^4 to $-6.0 \times 10^3 \text{ m}^3/\text{year}$. However, it may be inappropriate to apply a point pressure source model, because the estimated model has a very shallow underground distribution, and it may not be deformed as an elastic body. Modeling that takes into account the physical properties of the ground is a future issue. At a minimum, the modeling results suggest that the cause of subsidence may be due to very shallow contraction, possibly several hundred meters below the ground surface.

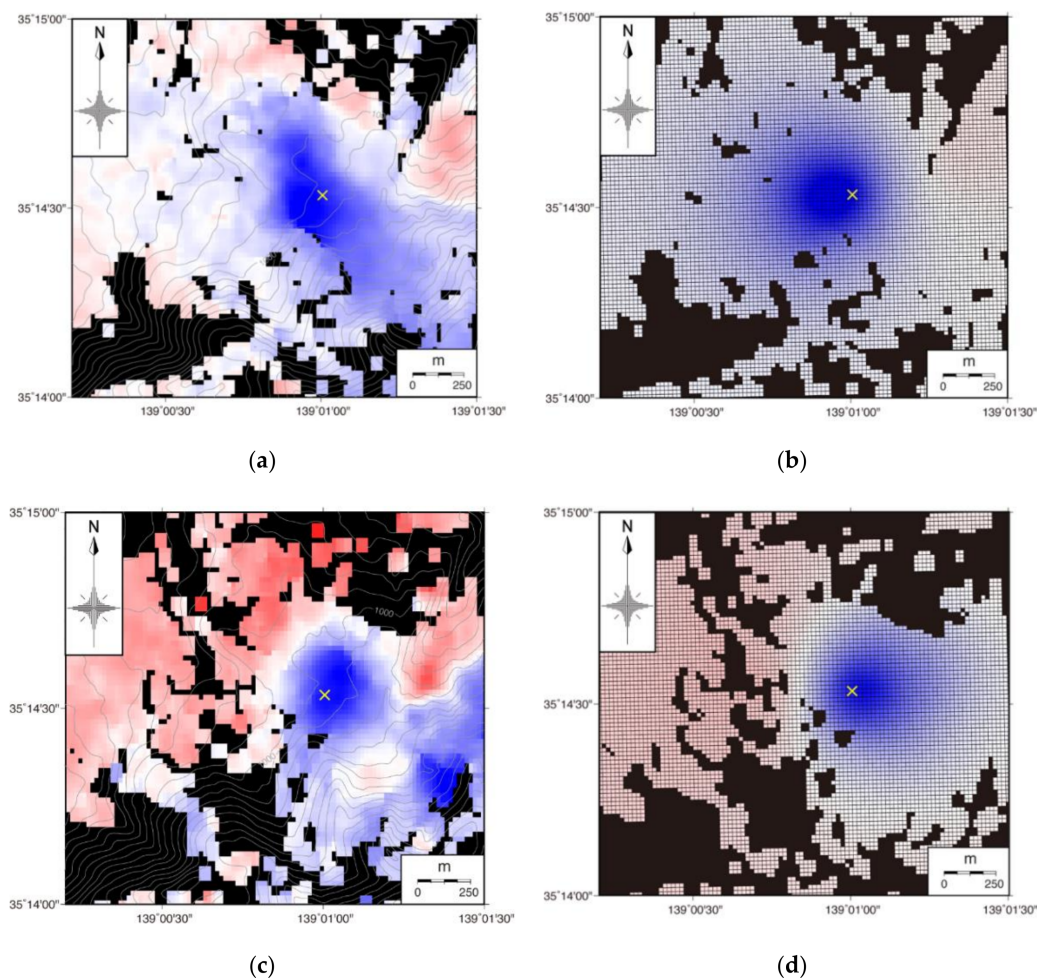


Figure 10. Results of the inversion analysis for estimating the point pressure source beneath the ground surface to the west of Owakudani: (a) observed velocity in the ascending orbit; (b) simulated velocity in the ascending orbit; (c) observed velocity in the descending orbit; (d) simulated velocity in the descending orbit. Contour lines in (a,c), in which intervals are 25 m, were extracted from 10 m mesh height data released by the GSI. The yellow “x” marks the location of the point pressure source, the parameters of which are shown in Table 2. Estimated offsets for the ascending and descending orbits are +0.15 and +2.43 mm/year, respectively. The color scales used for the velocity are the same as those in Figures 5 and 6.

Table 2. Estimated parameters of the point pressure source beneath the area of subsidence to the west of Owakudani.

Volume Variation (m ³ /year)	Altitude (m) ¹	East(°) ²	North(°) ²
-1.04×10^4	701.6	139.016746	35.242233

¹ Altitude is the height above sea level. ² Coordinates are in WGS84 format.

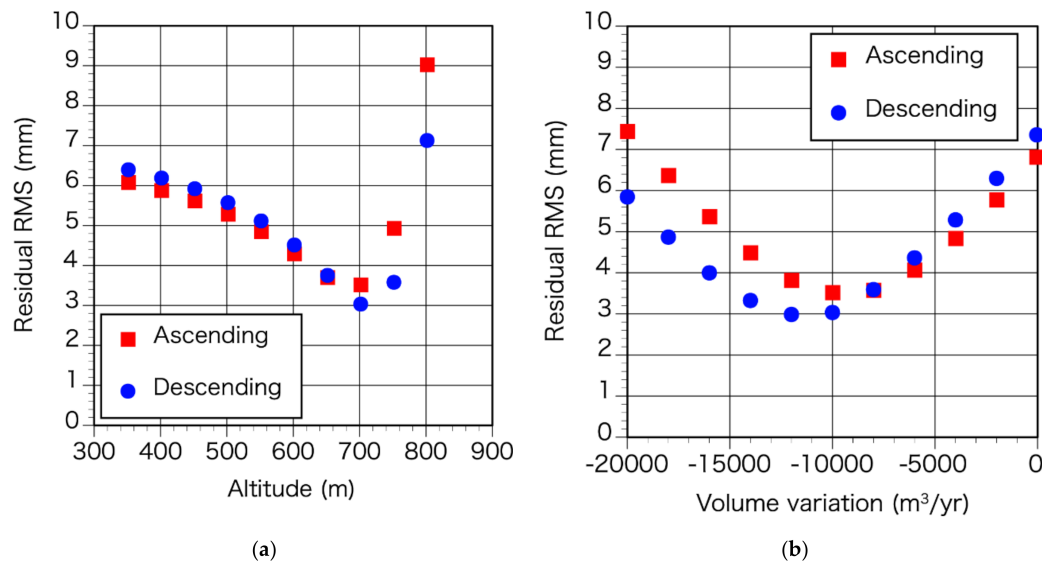


Figure 11. Residual root mean square (RMS) values estimated by forward modeling and varying (a) altitude and (b) volume variation. Altitude and volume variation changes every 50 m and 2000 m³/year, respectively. During forward modeling, the other parameters were held at optimum values (Table 2).

4. Discussion

Hot spring wells have been developed in the Owakudani region for decades, and many of these wells are located to the east of the subsidence area. Most of the hot spring wells in Owakudani are steam wells; hot water for bathing is artificially produced by adding local groundwater to the self-discharged volcanic steam that comes up from boreholes, which are several hundred meters in depth. The hot water produced by steam wells in Owakudani is acidic with high concentrations of chloride ions, which are derived from a magma activity of about 10 km in depth [22,23].

On the other hand, in the western region of Owakudani, most of the hot spring water is drawn from the wells. These hot spring waters contain primarily sulfate and bicarbonate, which are naturally produced by volcanic gas added to groundwater distributed near the surface, except for well MO39 (Figures 12 and 13). The hot spring well MO39, which is closest to the area of subsidence, is a steam well that produces acidic spring water from self-discharged volcanic steam with chloride ions as its main dissolved chemical component (Figure 13).

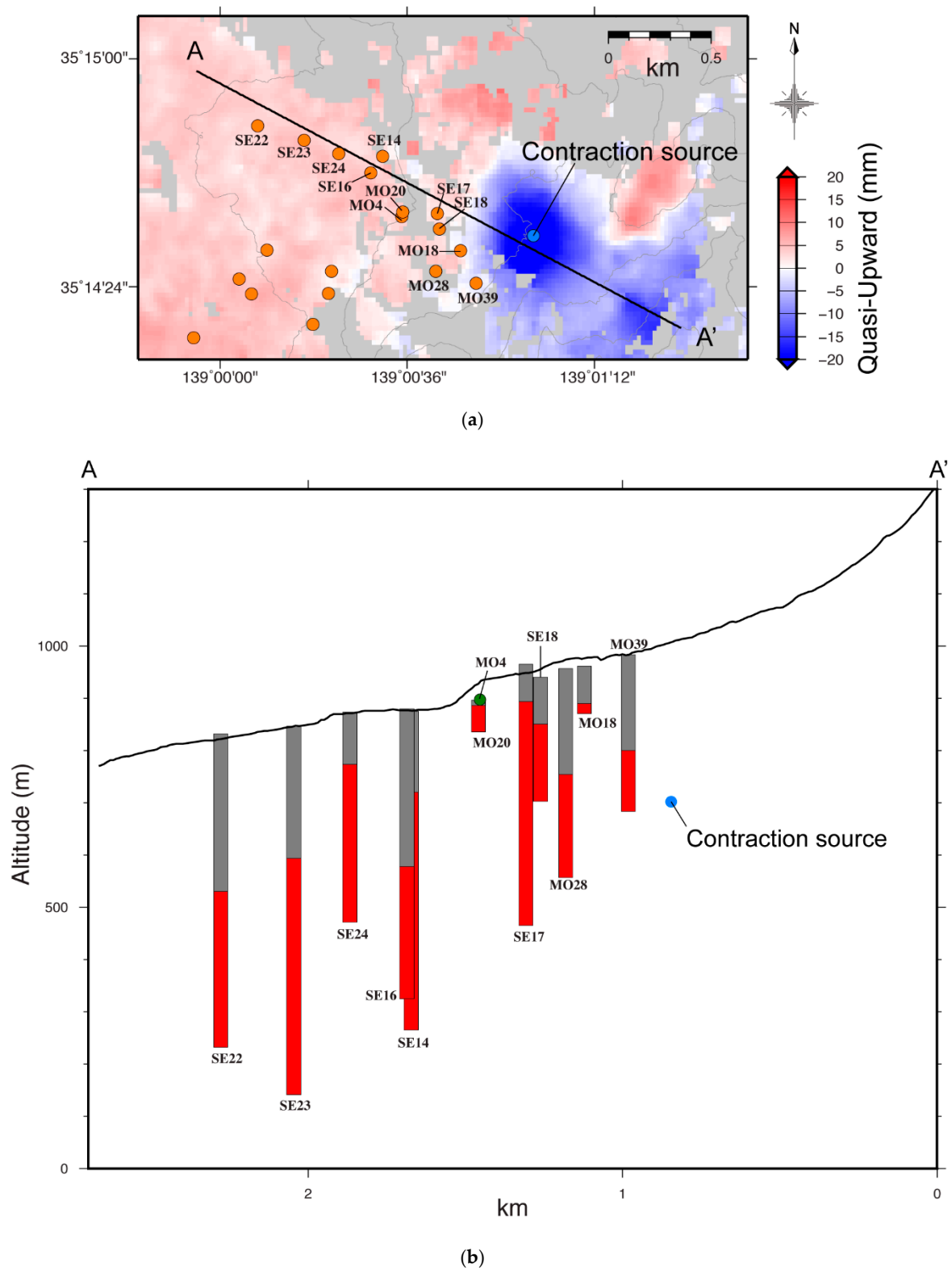


Figure 12. Characteristics of the hot spring wells to the west of Owakudani as (a) a horizontal distribution of hot spring wells (orange-colored points) on the map of quasi-upward velocity; (b) cross-section indicated by A-A' in (a). Contour lines in (a), in which intervals are 100 m, were extracted from 10 m mesh height data released by the GSI. MO (Motohakone) and SE (Sengokuhara) indicate the numbers of hot spring wells managed by the Odawara Health and Welfare Office. Gray and red colors in (b) show the extent of cased and uncased parts of the borehole, respectively. MO4 is a natural hot spring at the surface.

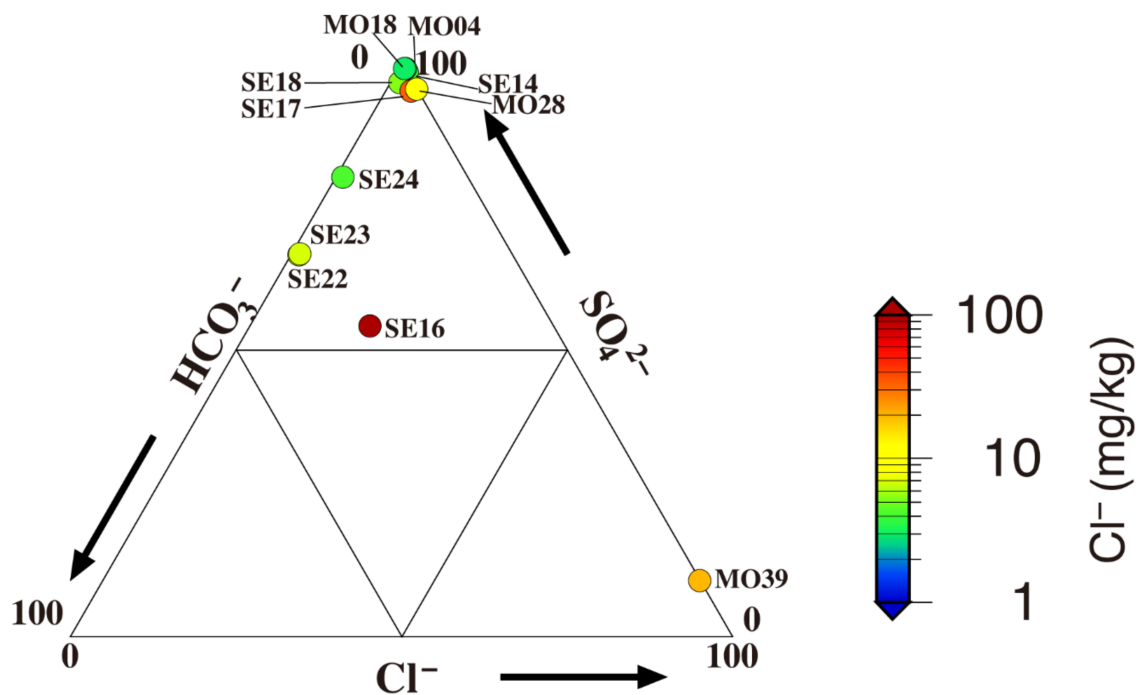


Figure 13. Triangular plot of major anions in hot spring water from wells to the west of Owakudani. The numbers in the triangular plot indicate the composition (%) of each ion. The colored circles show the chloride ion content in the hot spring water. The numbers of the hot spring wells and their locations are shown in Figure 12.

Figure 12 shows the depth and characteristics of the hot spring wells to the west of Owakudani. To prevent cold water from mixing with the hot spring water, casing pipes are typically installed from the top of the well to a certain depth in the wells. The casing pipes allow for the collection of the hot spring water or steam directly from the depth of the uncased part of the borehole, where the hot spring aquifers are exposed. Based on the structure of the wells to the west of Owakudani, hot spring water, or steam is collected from around 600–800 m above sea level (Figure 12). These data indicate that the hot spring water or steam in this region is distributed at a depth of several hundred meters below the ground surface. Interestingly, the contraction source estimated by this study is also located at a depth of several hundred meters, which is almost coincident with the hot spring source. Therefore, the subsidence observed in the area is considered to be due to the contraction of the reservoir from which the hydrothermal fluids are being supplied from below.

So, what has caused this reservoir contraction? The Owakudani fumaroles, which is located a few hundred meters east of the area of subsidence, are more active than the fumaroles to the west of Owakudani (Figure 14). In Owakudani, an area 200 m in diameter was locally uplifted during volcanic unrest in 2015, and a phreatic eruption occurred in the vicinity of the uplifted area [7,24]. This local uplifting was explained by expansion sources approximately 80–150 m below the ground surface [7,24]. This expansion suggests the existence of a reservoir that supplies hydrothermal fluids and causes the fumarolic activity on the surface of Owakudani. The hydrothermal fluids with highly concentrated chloride ions are considered to be directly supplied to this reservoir through cracks from the deeper parts of the volcano [7].

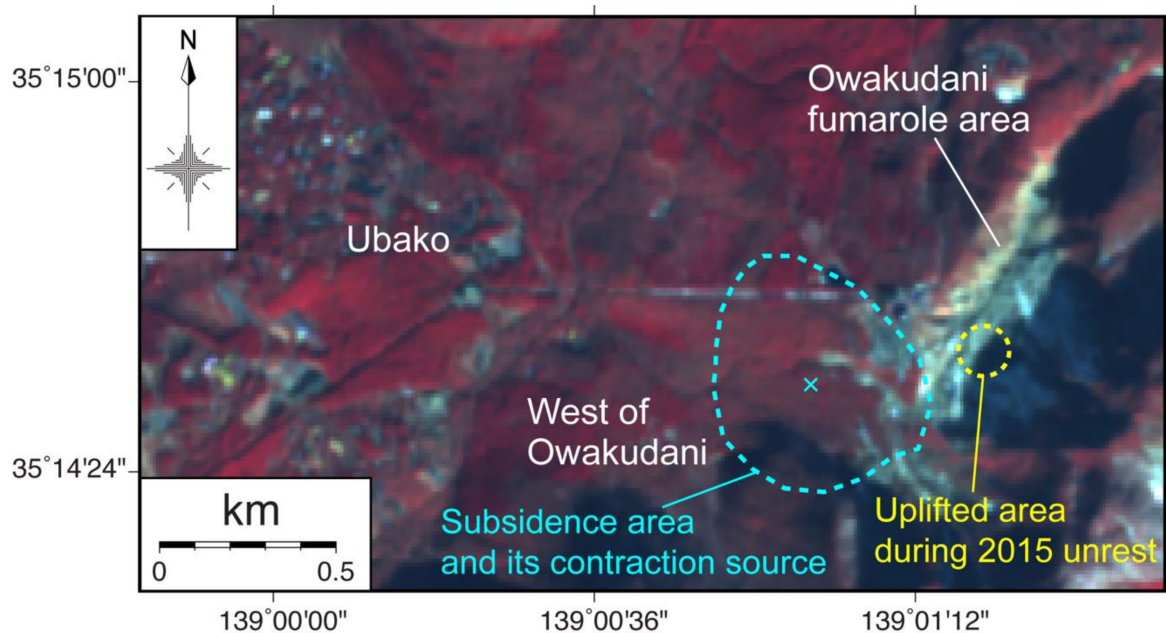


Figure 14. False-color image around the Owakudani fumarole area captured by ALOS/AVNIR-2 on 31 January 2007. The red color in the image indicates areas of vegetation, and in the Owakudani fumarole area, there is no vegetation due to geothermal and fumarolic activity.

Conversely, there are no such active fumaroles to the west of Owakudani, where the subsidence was observed (Figure 14), although there are small fumarolic activities that make a discharge. However, in 1872, the French engineer Jean-Paul Ishidor Vidal is on record as having measured the temperature of the steam in the western area of Owakudani as 103 °C [5,25,26]. This implies that the area of subsidence was once a fumarole zone with heated steam. Moreover, chloride ion that is contained as a major anion in hot spring water of MO39 (Figure 13), which is the closest to the area of subsidence, is implying the participation of the hydrothermal fluids supplied directly from the deeper parts of the volcano [22]. This suggests that the observed subsidence is associated with attenuation of fumarole activity in response to a decrease in the supply of hydrothermal fluids from below. It is also possible that this attenuation may have arisen due to closure of the fluid path from deeper regions, such as a crack. Another possible cause of subsidence may be excessive pumping of hot spring water. However, MO39, the well closest to the subsidence area, is a steam well and uses self-discharged steam, not artificially pumping hot spring water. It is not considered that forced dissipation of pore water pressure, such as land subsidence resulting from excessive groundwater pumping, has occurred. To accurately clarify these factors, it will be necessary to continuously monitor the discharge volume and temperature of the hot spring water.

In this study, we used SAR data acquired by the ALOS/PALSAR satellite from 2006 to 2011. After the termination of ALOS/PALSAR in 2011, the ALOS-2/PALSAR-2 satellite was launched. We consider it essential to continue monitoring the surface displacement in the area to the west of Owakudani to clarify whether the subsidence is continuing or not; this will form part of future studies.

5. Conclusions

Based on an SBAS-InSAR time series analysis, we observed highly localized subsidence in an area to the west of Owakudani in the Hakone Volcano, Japan, from 2006 to 2011 using ALOS/PALSAR data. The area of subsidence was approximately 500 m in diameter, and the peak rate of subsidence was approximately 25 mm/year. The results of point pressure source modeling suggested that the cause of the observed subsidence was due to reservoir contraction at approximately 700 m above sea level (about 300 m below the ground surface). The rate of contraction was estimated to be $1.04 \times 10^4 \text{ m}^3/\text{year}$.

Based on the structure of the hot spring wells and their chemical components, the contraction source is considered to be a reservoir containing hydrothermal fluids. Moreover, the subsidence suggests that the attenuation of fumarole activity is occurring due to a decrease in hydrothermal fluid supply.

In addition, the findings of this study demonstrated the application of InSAR surface displacement measurements to monitor hydrothermal activity in shallow parts of volcanic areas. Monitoring surface displacement is considered useful, not only for evaluating the potential occurrence of phreatic eruptions but also for clarifying the production mechanism of hot spring water in volcanic regions.

Author Contributions: Conceptualization, R.D.; methodology, R.D.; validation, R.D.; formal analysis, R.D.; investigation, R.D.; data curation, R.D. and G.K.; writing—original draft preparation, R.D.; writing—revision and editing, R.D., G.K. and K.I.; visualization, R.D. and K.I.; funding acquisition, R.D. All authors have read and agreed to the published version of the manuscript.

Funding: This research was funded by JSPS KAKENHI, grant number 19K04005.

Acknowledgments: We thank Teruyuki Kato for his useful comments and encouragement. We also thank editors and three anonymous reviewers for their constructive comments. ALOS/PALSAR and AVNIR-2 data were provided by JAXA via the Coordinating Committee for the Prediction of Volcanic Eruption as part of the project “ALOS Domestic Demonstration on Disaster Management Application” of the Volcano Working Group. The original ALOS/PALSAR and AVNIR-2 data belong to JAXA/Ministry of Economy, Trade and Industry (METI). The daily coordinates of GNSS sites were obtained through GSI. We used Generic Mapping Tools [27] to draw the figures.

Conflicts of Interest: The authors declare no conflict of interest.

References

1. Sato, C.; Haga, M.; Nishino, J. Land subsidence and groundwater management in Tokyo. *Int. Rev. Environ. Strateg.* **2006**, *6*, 403–424.
2. Zhou, C.; Gong, H.; Chen, B.; Gao, M.; Cao, Q.; Cao, J.; Duan, L.; Zuo, J.; Shi, M. Land subsidence response to different land use types and water resource utilization in Beijing-Tianjin-Hebei, China. *Remote Sens.* **2020**, *12*, 457. [[CrossRef](#)]
3. Matsuda, T. Collision of the Izu-Bonin Arc with Central Honshu: Cenozoic tectonics of the Fossa Magna, Japan. *J. Phys. Earth* **1978**, *26*, S409–S420. [[CrossRef](#)]
4. Geological Society of Japan Eds. *Geological leaflet 1 Hakone Volcano*; Geological Society of Japan: Tokyo, Japan, 2007. (In Japanese)
5. Mannen, K.; Yukutake, Y.; Kikugawa, G.; Harada, M.; Itadera, K.; Takenaka, J. Chronology of the 2015 eruption of Hakone volcano, Japan: Geological background, mechanism of volcanic unrest and disaster mitigation measures during the crisis. *Earth Planets Space* **2018**, *70*, 68. [[CrossRef](#)]
6. Geological Survey of Japan, AIST Eds. *Seamless Digital Geological Map of Japan 1: 200,000. May 29, 2015 Version*; Geological Survey of Japan, National Institute of Advanced Industrial Science and Technology: Tukuba, Japan, 2015.
7. Doke, R.; Harada, M.; Mannen, K.; Itadera, K.; Takenaka, J. InSAR analysis for detecting the route of hydrothermal fluid to the surface during the 2015 phreatic eruption of Hakone Volcano, Japan. *Earth Planets Space* **2018**, *70*, 63. [[CrossRef](#)]
8. Yukutake, Y.; Ito, H.; Honda, R.; Harada, M.; Tanada, T.; Yoshida, A. Fluid-induced swarm earthquake sequence revealed by precisely determined hypocenters and focal mechanisms in the 2009 activity at Hakone volcano, Japan. *J. Geophys. Res.* **2011**, *116*, B4. [[CrossRef](#)]
9. Oki, Y.; Hirano, T. The geothermal system of the Hakone volcano. *Geothermics* **1970**, *2*, 1157–1166. [[CrossRef](#)]
10. Berardino, P.; Fornaro, G.; Lanari, R.; Sansosti, E. A new algorithm for surface deformation monitoring based on small baseline differential SAR interferograms. *IEEE Trans. Geosci. Remote Sens.* **2002**, *40*, 2375–2383. [[CrossRef](#)]
11. Rosenqvist, A.; Shimada, M.; Ito, N.; Watanabe, M. ALOS PALSAR: A Pathfinder mission for global-scale monitoring of the environment. *IEEE Trans. Geosci. Remote Sens.* **2007**, *45*, 3307–3316. [[CrossRef](#)]
12. Pavlis, N.K.; Holmes, S.A.; Kenyon, S.C.; Factor, J.K. The development and evaluation of the Earth Gravitational Model 2008 (EGM2008). *J. Geophys. Res. Solid Earth* **2012**, *117*, B4. [[CrossRef](#)]

13. Goldstein, R.M.; Werner, C.L. Radar interferogram filtering for geophysical applications. *Geophys. Res. Lett.* **1998**, *25*, 4035–4038. [[CrossRef](#)]
14. Costantini, M. A novel phase unwrapping method based on network programming. *IEEE Trans. Geosci. Remote Sens.* **1998**, *36*, 813–821. [[CrossRef](#)]
15. Fujiwara, S.; Nishimura, T.; Murakami, M.; Nakagawa, H.; Tobita, M.; Rosen, P.A. 2.5-D surface deformation of M6.1 earthquake near Mt Iwate detected by SAR interferometry. *Geophys. Res. Lett.* **2000**, *27*, 2049–2052. [[CrossRef](#)]
16. Sagiya, T. A decade of GEONET: 1994–2003—The continuous GPS observation in Japan and its impact on earthquake studies. *Earth Planets Space* **2004**, *56*, 8. [[CrossRef](#)]
17. Hao, M.; Li, Y.; Zhuang, W. Crustal movement and strain distribution in East Asia revealed by GPS observations. *Sci. Rep.* **2019**, *9*, 16797. [[CrossRef](#)]
18. Harada, M.; Hosono, K.; Kobayashi, A.; Yukutake, Y.; Yoshida, A. Extensional strains around Mt. Fuji and Hakone Volcano and low-frequency earthquakes. *Bull. Volcanol. Soc. Jpn.* **2010**, *55*, 193–199. (In Japanese with English abstract) [[CrossRef](#)]
19. Mitsui, Y.; Kato, T. Magmatic inflation in 2008–2010 at Mt. Fuji, Japan, inferred from sparsity-promoting L1 inversion of GNSS data. *J. Volcanol. Geotherm. Res.* **2019**, *378*, 29–34. [[CrossRef](#)]
20. Mogi, K. Relations between the eruptions of various volcanoes and the deformations of the ground surfaces around them. *Bull. Earthq. Res. Inst.* **1958**, *36*, 99–134.
21. Marquardt, D.W. An algorithm for least-squares estimation of nonlinear parameters. *J. Soc. Ind. Appl. Math.* **1963**, *11*, 431–441. [[CrossRef](#)]
22. Ohsawa, S.; Yusa, Y.; Oyama, M. Information of geothermal system beneath Hakone Volcano, Japan, obtained by chemical compositions of discharged gases. *J. Hot Spring Sci.* **2000**, *49*, 151–161. (In Japanese with English abstract)
23. Yukutake, Y.; Honda, R.; Harada, M.; Arai, R.; Matsubara, M. A magma-hydrothermal system beneath Hakone volcano, central Japan, revealed by highly resolved velocity structures. *J. Geophys. Res. Solid Earth* **2015**, *120*, 3293–3308. [[CrossRef](#)]
24. Kobayashi, T.; Morishita, Y.; Munekane, H. First detection of precursory ground inflation of a small phreatic eruption by InSAR. *Earth Planet. Sci. Lett.* **2018**, *491*, 244–254. [[CrossRef](#)]
25. Sunaga, T. Vidal’s Hakone and Atami Onsen travelogue—A French doctor’s survey of the hot springs in 1872. *Onsen* **2003**, *71*, 4–12. (In Japanese and title was translated)
26. Mannen, K. Overheated steams in Owakidani fumarolic area; history and cause of extinction. *Bull. Hot Springs Res. Inst. Kanagawa Prefect.* **2009**, *41*, 23–32. (In Japanese with English abstract)
27. Wessel, P.; Smith, W.H.F.; Scharroo, R.; Luis, J.; Wobbe, F. Generic mapping tools: Improved version released. *Eos Trans. Am. Geophys. Union* **2013**, *94*, 409–410. [[CrossRef](#)]

